PCCP

Accepted Manuscript

ROYAL SOCIETY OF CHEMISTRY

www.rsc.org/pccp

PCCP

RSCPublishing

ARTICLE

Particle size dependence of the surface-enhanced Raman scattering properties of densely arranged two-dimensional assemblies of Au(core)-Ag(shell) nanospheres

Cite this: DOI: 10.1039/xoxxoooooox

Received ooth January 2012,
Accepted ooth January 2012

DOI: 10.1039/xoxxoooooox

www.rsc.org/

Kosuke Sugawa,[*a] Tsuyoshi Akiyama,[*b] Yoshimasa Tanoue,[a] Takashi Harumoto,[c] Sayaka Yanagida,[d] Atsuo Yasumori,[c] Shohei Tomita,[c] Joe Otsuki[a]

We investigated the dependence of the surface-enhanced Raman scattering (SERS) activity of densely arranged two-dimensional assemblies of spherical Au(core)-Ag(shell) nanoparticles (Au/AgNSs) on the nanoparticle diameter. The size-controlled Au/AgNSs were synthesized using the Au nanosphere seed-mediated growth method without any bulky stabilizers. The diameters of the Au/AgNSs were 38, 53, and 90 nm and the ratio of the total diameter to the Au core diameter was adjusted to *ca.* 2.0. Extinction spectra of the colloidal solutions of these nanoparticles exhibited the prominent peak of the localized surface plasmon resonance (LSPR) of Ag and therefore the Au/AgNSs exhibited LSPR properties almost the same as Ag nanospheres. It was confirmed from SEM observation that the organic solvent-mediated liquid-liquid interface assembly technique easily generated densely arranged two-dimensional assemblies of the nanospheres. The extinction spectra of all the assemblies exhibited a prominent broad peak ranging from 500 nm to the near-infrared region, which is assigned to the longitudinal LSPR mode of the coupling nanospheres. The extinction intensity increased with increasing nanosphere diameter. The SERS activities of these assemblies were investigated using *p*-aminothiophenol as a probe molecule. The result revealed that the enhancement factor (EF) of the Raman signal dramatically increased with increasing the particle diameter. The maximum EF obtained with a laser excitation wavelength of 785 nm was 1.90×10^6 for a nanosphere diameter of 90 nm. This renders the two-dimensional assemblies of the plasmonic Au/AgNSs promising for the development of highly sensitive SERS sensor platforms due to their strong electromagnetic effect.

1. Introduction

Surface-enhanced Raman scattering (SERS) has emerged as a uniquely-sensitive molecular fingerprinting technique, which is applicable in the fields of medical science, life sciences, and analytical chemistry.[1] It has been found that when molecules come close to Au and Ag nanoparticles, the Raman signal is enhanced on the order of 10^4-10^6.[2] Recently, the detection of single molecules with SERS has been reported.[3] Although the exact mechanism for signal enhancement in SERS has been a matter of considerable debate, it is generally considered to be due to the two distinct mechanisms.[4] The first one ascribes the signal enhancement to a drastic enhancement in the electromagnetic fields generated by the excitation of localized surface plasmon resonance (LSPR) in the vicinity of metal nanostructures (electromagnetic effect). The second one posits the formation of charge transfer complexes between the adsorbed molecules and the surfaces of the metal nanostructures (chemical effect). It has been reported that the chemical effect can enhance the Raman signal up to 10-10^3 times, whereas the electromagnetic effects can result in an enhancement up to 10^{10}-10^{12} times.[5] Therefore, the fabrication of plasmonic metal nanostructures that generate strong local electromagnetic fields for a strong electromagnetic effect is a milestone toward the development of highly active SERS platforms.

Against this background, it has recently been demonstrated that the formation of "hot spots" is important for the generation of a high SERS activity. Hot spots are induced by the LSPR coupling between adjacent metal nanoparticles and produce drastically amplified electromagnetic fields in the gap region. As a result, these unique local fields can significantly enhance the Raman signals to an extent that enables the monitoring of molecular structures at the single molecule level.[3,6] Although Au, Ag, and Cu have frequently been used for the generation of SERS, Ag, in particular, has been believed to played the most important role in the development of SERS platforms since Ag LSPR produces much stronger electromagnetic fields in the visible region than Au and Cu.[7]

As one of the highly active SERS platforms, densely arranged two-dimensional (2-D) assemblies of Ag nanoparticles have previously been reported.[8-12] The close proximity of adjacent nanoparticles is expected to generate multiple hot spots on these assemblies, resulting in high SERS activities. These assemblies have been previously fabricated by vacuum evaporation[8], the Langmuir-Blodgett (LB) technique[9], and the layer-by-layer (LBL) assembly method.[10] However, these methods are time-consuming and/or require special apparatuses. Furthermore, bulky polymer stabilizers such as polyvinylpyrrolidone, which are used to protect the nanoparticles in the LB technique, cannot be compatible with the practical SERS platforms since they will prevent the adsorption of analyte molecules on the nanoparticle surfaces. On the other hand, we recently succeeded in fabricating the densely arranged 2-D assemblies of Ag nanospheres with a diameter of about 72 nm by self-assembling the nanospheres at liquid-liquid interfaces.[11] This is a simple and rapid method, which leads to the formation of densely arranged 2-D assemblies over large areas without the use of any bulky stabilizers and special apparatuses. In addition, we found that these assemblies can act as excellent SERS platforms since the Raman signals of the immobilized probe molecule (*p*-aminothiophenol: PATP) were strongly enhanced due to the generation of hot spots.

Despite these progresses, the influence of the diameter of assembled Ag nanospheres on the SERS activity has never been investigated, although the optimal diameter of Ag nanospheres, which were bound in complexes with probe molecules, well-dispersed in the liquid phases has been studied.[13] In our previous report, the Ag nanoparticles were synthesized by the citric acid reduction method, with which it is difficult to precisely control the particle diameter. In addition, Ag nanowires and nanorods byproducts were partly contained in the colloidal solution and the resultant assemblies.[11] Therefore, it was impossible to address the effects of particle diameter on the SERS activity. The dependence of the SERS effect of the densely arranged 2-D assemblies on the Ag nanoparticle diameter may be different from that for the liquid phases since these two systems exhibit different optical properties and structural features. For example, densely arranged assemblies exhibit a prominent LSPR peak due to the generation of hot spots, which are not induced in dispersed nanospheres.[11] In addition, it must be noted that the density of the generated hot spots per unit area decreases with increasing the nanosphere diameter. Therefore, an experimental investigation of the diameter dependence of the SERS activity on the nanosphere diameter in 2-D assemblies is very important for the development of highly active SERS platforms.

Toward this purpose, we synthesized Au(core)-Ag(shell) type nanospheres (Au/AgNSs) as Ag-like nanospheres by a seed-mediated growth method from the Au nanospheres (AuNSs) as seeds.[13(a),14] The synthesis of precisely size-controlled silver nanospheres without any bulky stabilizers is still challenging.[15] On the other hand, controlling the diameter of the AuNSs is relatively easy and the monodispersity of the obtained nanoparticles is relatively high.[16] Therefore, the nanosphere diameter of the Au/AgNSs synthesized from the AuNSs can be easily adjusted. In this study, we fabricated the 2-D assemblies of Au/AgNSs with defined diameters and investigated their SERS activity in the hot spot wavelength region, where the coupling modes of the LSPRs are induced.[13(d)]

2. Experimental

2-1. Reagent

Deionized water (resistivity: 18.2 MΩ·cm), which was obtained from a Milli-Q water purification system, was used for the preparation of all aqueous solutions. Hydrogen tetrachloroaurate(III) tetrahydrate ($HAuCl_4 \cdot 4H_2O$; Nacalai Tesque), silver nitrate ($AgNO_3$; Wako Pure Chemicals), trisodium citrate dihydrate (Kanto Chemical), *p*-aminothiophenol (PATP; Tokyo Chemical Industry), L-ascorbic acid (Wako Pure Chemicals), *n*-hexane (Kishida Chemical), and methanol (Wako 1st Grade, Wako Pure Chemicals) were used as purchased without further purification.

2-2. Preparation of aqueous colloidal solutions of Au nanospheres and Au(core)-Ag(shell) nanospheres.

We synthesized aqueous colloidal solutions of AuNSs with three different diameters.[17] Typically, after refluxing an aqueous solution (100 mL) of 0.01 wt% tetrachloroauric(III) acid for 30 min, an aqueous solution (2.15 mL, 1.50 mL, and 0.90 mL) of 1 wt.% trisodium citrate dihydrate was injected into the solution, which was then refluxed for 60 min to produce an aqueous solution of AuNSs with diameters of 19 ± 1 nm (AuNS(19)), 27 ± 4 nm (AuNS(27)), and 46 ± 6 nm (AuNS(46)), respectively.

Aqueous colloidal solutions of Au/AgNSs with different diameters were prepared using the AuNS seeds-mediated growth method.[13(d)] Typically, the as-prepared aqueous colloidal solution of AuNSs (50 mL) and 0.1 M ascorbic acid (7.2 mL) were stirred vigorously in a 100 mL vial for 15 min. Next, an aqueous solution of 1 mM $AgNO_3$ was added dropwise to the solution. The radius ratio of Au/AgNSs to the AuNSs cores was adjusted to be approximately 2.0 for each nanoparticle solution by controlling the additive amount of the aqueous solution of $AgNO_3$ (AuNSs(19): 50 mL, AuNSs(27): 50 mL, and AuNSs(46): 54 mL). As a result, the diameters of Au/AgNSs synthesized from AuNSs (19, 27, and 46) were 38 ± 6 (Au/AgNS(38)), 53 ± 7 (Au/AgNS(53)), and 90 ± 10 nm (Au/AgNS(90)), respectively.

2-3. Fabrication of 2-D nanoparticle assemblies consisting of Au/AgNSs.

Scheme 1 depicts the fabrication of the Au/AgNSs assemblies by a modified organic solvent-mediated liquid-liquid interface assembly technique.[11,18] Briefly, an aqueous solution (200 μL) of 10 wt% trisodium citrate dihydrate was injected into the colloidal solution of Au/AgNSs and stirred for 15 s. Subsequently, hexane (2 mL) was added to this solution, resulting in the formation of an organic-aqueous interface in the sample vial. Then, 25 mL of methanol was vigorously injected into the colloidal solution. Immediately after this, liquid-like shiny films of Au/AgNSs were formed at the organic-aqueous interface. The hydrophilic glass plate was produced as follows. The glass plate was treated with a 1:1 (v/v) solution of NH_3 (aq. 28 %) and H_2O_2 (aq. 30 %) for 1 h at 100 °C, followed by washing with a sufficient amount of water. As the pretreated glass plate was placed onto the film formed at the interface, the films quickly and spontaneously deposited and formed Au/AgNSs assemblies on the glass surface.

2-4. Sample preparation for SERS studies

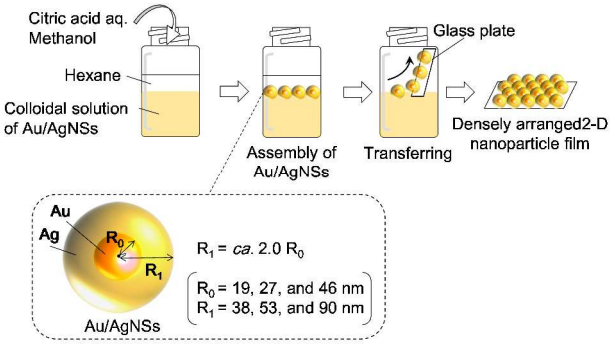

Scheme 1. Fabrication scheme of densely arranged two-dimensional assemblies of Au/AgNSs.

In order to evaluate the SERS activity of the resultant Au/AgNS assemblies, Raman scattering spectra were measured using PATP as a probe molecule.[19] The glass substrates modified with the Au/AgNSs assemblies were immersed into a methanol solution of PATP (1 mM) for 12 h. The well-known high chemical affinity between thiol groups and Ag lead to the formation of a monolayer of PATP molecules on the Au/AgNS assemblies.[20] Then the substrates were rinsed with methanol to ensure the desorption of non-specifically bound PATP.

2-5. Measurements

UV–Vis spectroscopy was carried out on a JASCO V-630 spectrophotometer. Field-emission scanning electron microscope (FE-SEM) images were taken with a Hitachi S-4500 microscope with an acceleration voltage of 15 kV. Transmission electron microscope (TEM) images were taken with a Hitachi HF-2000 with an acceleration voltage of 200 kV. Elemental mapping images and a high-angle annular dark-field scanning transmission electron microscopy (HAADF-STEM) images were taken with the scanning transmission electron microscope (STEM, HD-2300C, Hitachi) with energy dispersive X-ray spectrometer (EDS, EDAX). Raman scattering spectra of the PATP-modified nanosphere assemblies and reference solutions (methanol solution containing 10 M PATP) were obtained with a micro-Raman spectrometer (NRS-5100, JASCO). The excitation source was a CW laser with excitation wavelengths of 532 nm and 785 nm and powers of approximately 43 mW and 47 mW, respectively. The laser was focused onto the sample surfaces using an objective lens (100× magnification). In order to reduce the degradation of the samples, the excitation laser was passed through a neutral density filter. We proved that the stability of the Au/AgNSs assemblies was maintained during the SERS measurements: multiple measurements at the same measurement point did not cause any significant changes in the signal intensity.

3. Results and discussion

3-1. Morphological and optical characterization of AuNSs as cores and Au/AgNSs

In this study, we synthesized Au/AgNSs with various diameters using an AuNS seed-growth method. The nanospheres were stabilized using only a small molecule (citric acid). This is crucial for the development of SERS platforms since bulky stabilizers may hinder the adsorption of analyte

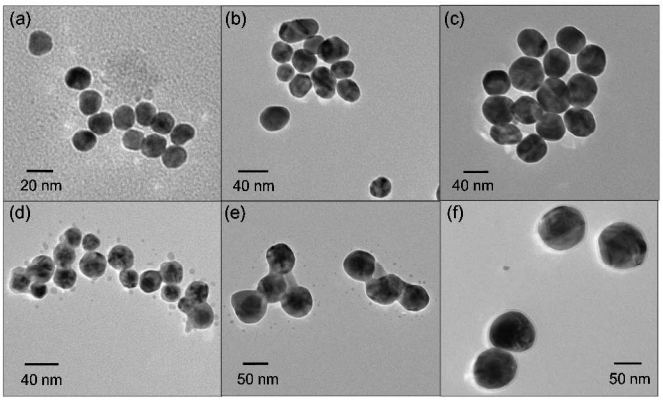

Figure 1. TEM images of (a) AuNS(19), (b) AuNS(27), (c) AuNS(46), (d) Au/AgNS(38), (e) Au/AgNS(53), and (f) Au/AgNS(90).

molecules on the nanosphere surfaces. Average nanosphere sizes of the synthesized AuNSs and Au/AgNSs were estimated from their TEM images. Control of the AuNS diameters was achieved by controlling the additive amount of the aqueous solution of citric acid, which acted as a reducing and protecting agent in the synthesis process. Typically, decreasing the additive amount of citric acid solution resulted in an increase in the particle diameters of the resultant AuNSs.[17,21] As a result, we obtained three kinds of AuNSs with the diameters of 19 ± 1, 27 ± 4, and 46 ± 6 nm, as shown in Figure 1 (a)-(c).

In order to mostly generate the Ag-derived LSPR of the Au/AgNSs, we adjusted the radius ratio of the Au/AgNSs to the AuNS cores to approximately 2.0 for each nanoparticle size by controlling the additive amount of the aqueous $AgNO_3$ solution that was injected into the solution containing the AuNSs and ascorbic acid as a reducing agent. The diameters of the formed Au/AgNSs were 38 ± 6, 53 ± 7, and 90 ± 10 nm for AuNS(19), AuNS(27), and AuNS(46), respectively ((d)-(f) in Figure 1). In order to investigate their morphological characterization, HAADF images of Au/AgNSs were measured (Figure 2). The outer shell region is significantly darker, as compared with the core region, which indicates the presence of a high-Z element at the cores and low-Z element at the shells, which are Au and Ag, respectively in the present case. In the case of Au/AgNS(90), a hollow gap is seen between the Au core and the Ag shell, which we cannot explain at this stage. The mapping images of the Au M-edge and the Ag L-edge of Au/AgNS(90) obtained by the energy dispersive X-ray spectroscopy (EDS) analysis are shown in Figure 3. From these results, it was confirmed the presence of a Ag shell surrounding the Au core, which proves that the generated nanospheres exhibit the Au(core)-Ag(shell) morphology.

Extinction spectra of the aqueous colloidal solutions of AuNSs are shown in Figure 4(A). Each of the solutions of the AuNS(19), AuNS(27), and AuNS(46) exhibits a prominent peak at 524, 528, and 530 nm, which is ascribed to the dipole mode of the respective Au LSPR. The LSPR peak gradually red-shifts and broadens with increasing particle diameter. This is possibly due to depolarization and radiative damping effects, which arise from the finite size of the nanoparticles relative to the wavelength.[22] On the other hand, the optical properties of the colloidal solutions dramatically changed after deposition of the Ag shells around the Au core, as shown in Figure 4(B).

First, all of the aqueous colloidal solutions of Au/AgNSs show an

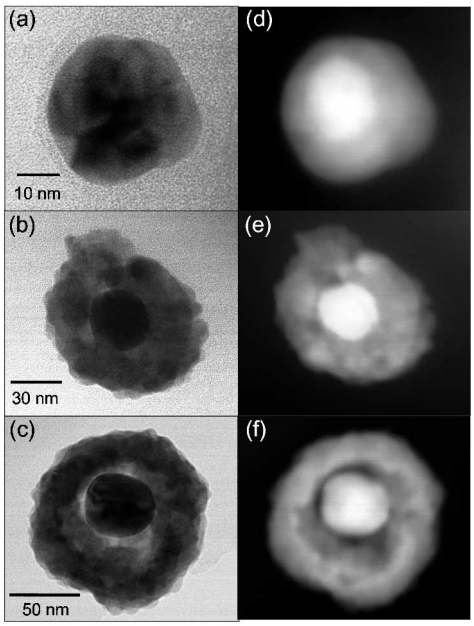

Figure 2. Bright field (BF)-STEM images of (a) Au/AgNS(38), (b) Au/AgNS(53), and (c) Au/AgNS(90). HAADF-STEM image of (d) Au/AgNS(38), (e) Au/AgNS(53), and (f) Au/AgNS(90).

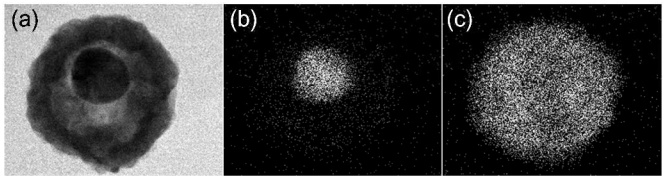

Figure 3. BF-STEM image and EDS elemental mapping images of Au/AgNS(90); (a) BF-STEM image; (b) EDS elemental mapping image of the Au M-edge; (c) EDS elemental mapping image of Ag L-edge.

absorption minimum around 325 nm. This is a specific optical characteristic of the plasmonic Ag nanospheres because this can be observed by overlapping the Ag interband transition with the Ag LSPR absorption.[23] Second, the shoulder peak around 350 nm, which is derived from the quadrupole mode of the Ag LSPR, clearly develops with increasing the total diameter (especially in Au/AgNS(90)).[22(d)] Finally, while the Au LSPR peak was almost screened by the Ag shells around the AuNSs, a new LSPR peak caused by the dipole mode of the Ag LSPR appeared at 399, 414, and 450 nm for Au/AgNS(38), Au/AgNS(53), and Au/AgNS(90), respectively.[22(d),23] The new LSPR peak gradually red-shifts and broadens with increasing total particle diameter, due to the same reasons applied in the case of the AuNSs (depolarization and radiative damping effect). These results confirm that the optical properties of the resultant Au/AgNSs are very similar to those of pure Ag nanospheres. Therefore, the hollow gaps, which were seen in Au/AgNS(90) in Figure 2, have little effect on the LSPR properties. It can be noted that the variation in the extinction intensity for the solution of AuNSs and Au/AgNSs does not reflect the diameter dependent LSPR properties, because the number of the nanoparticles contained in the sample may differ each other.

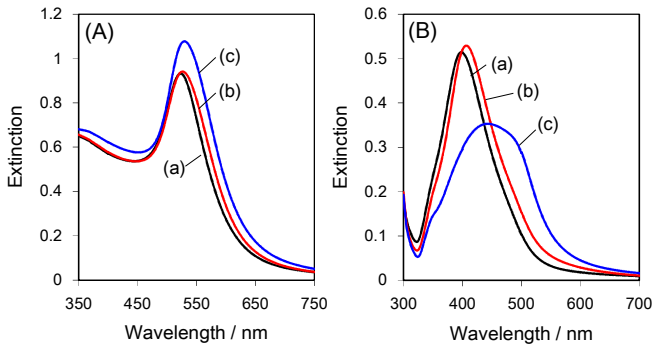

Figure 4. Extinction spectra of the aqueous colloidal solutions of (A) the core particles of (a) AuNS(19), (b) AuNS(27), and (c) AuNS(46) and (B) the corresponding core-shell particles of (a) Au/AgNS(38), (b) Au/AgNS(53), and (c) Au/AgNS(90).

3-2. Morphological and optical characterization of 2-D assemblies of Au/AgNPs

The densely arranged 2-D assemblies of the Au/AgNSs were fabricated from their aqueous colloidal solutions by an organic solvent-mediated liquid-liquid interface assembly technique.[11,18] Figure 5(A) (a)-(c) show photographs, which were taken immediately after vigorously injecting methanol into the biphasic solutions containing hexane and an aqueous colloidal solution. They clearly show the formation of nanosphere films with a shiny pale yellow color at the liquid-liquid interfaces in all of the colloidal solutions. These films were easily transferred onto the glass plates with hydrophilic surfaces, which were subsequently air-dried. As a result, uniform assemblies over the whole glass substrates were obtained, as shown in the photographs in Figure 5(B) (a)-(c). SEM images were taken in order to evaluate the microscopic morphology of the assemblies (see Figure 6). The formation of densely arranged nanoparticle assemblies is clearly visible from the top views. The cross-sectional views furthermore demonstrated that the nanoparticles mostly assemble in monolayers. The coverages were calculated to be 89, 87, and 86 % for Au/AgNS(38), Au/AgNS(53), and Au/AgNS(90), respectively, using the software ImageJ.[24] These values are close to that for close-packed structures (*ca.* 91 %).

Extinction spectra were recorded in order to evaluate the optical properties of the nanosphere assemblies (Figure 7). While all of the assemblies exhibit similar basic characteristics, they were substantially different from those of the colloidal Au/AgNS solutions (Figure 4 (B)). In addition, the extinction spectra were very similar to those of dense multilayer assemblies of pure Ag nanospheres fabricated by the LBL method.[25] This suggests that the formed Au/AgNS assemblies have the same LSPR properties as those of the assemblies of pure Ag nanospheres. In particular, all the spectra exhibit a relatively sharp extinction peak around 390 nm and a very broad extinction ranging from 500 nm to the near-infrared region. The former peak can be largely attributed to the LSPR mode of isolated individual Ag nanospheres but also appears to have contributions partly from the transverse LSPR mode of the coupling nanospheres. The latter in the longer wavelength region can be assigned to the longitudinal LSPR mode of the

coupling nanospheres.[25] Previous reports frequently suggest that the coupling between adjacent plasmonic nanoparticles induces extremely intense local electromagnetic fields, known

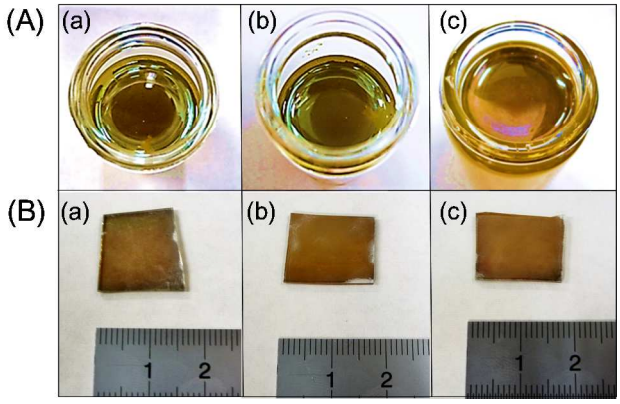

Figure 5. (A) Photographs of assemblies at the hexane-aqueous solution interface of (a) Au/AgNS(38), (b) Au/AgNS(53), and (c) Au/AgNS(90) and (B) photographs of the resultant assemblies consisting of (a) Au/AgNS(38), (b) Au/AgNS(53), and (c) Au/AgNS(90) on glass plates.

as "hot spots".[7,26] Therefore, our Au/AgNS assemblies hold promise as excellent SERS platforms due to the appearance of strong electromagnetic effects.[26]

3-3. SERS properties on Au/AgNSs assemblies

The SERS properties of the 2-D assemblies of the Au/AgNS(38), Au/AgNS(53), and Au/AgNS(90) were studied using PATP as a probe molecule. PATP adsorbs strongly onto the metal surfaces by forming stable metal-sulfur bonds and produces strong SERS signals, which are sensitive to the properties of the metal substrates.[19]

Figure 8(A) shows the SERS spectra (excitation laser wavelength: 532 nm) of Au/AgNSs assemblies with adsorbed PATP. The SERS signals of PATP can be detected for all of the assemblies. We observed peaks at 1068, 1137, 1183, 1384, and 1428 cm^{-1}. Conventionally, the prominent peaks at 1428, 1384, and 1137 cm^{-1} have been assigned to the non-totally symmetric b_2 modes and the peaks at 1183 and 1068 cm^{-1} have been assigned to the totally symmetric a_1 modes of PATP.[27] Moreover, the broad peak at around 1570 cm^{-1} have been ascribed to the overlay of the two peaks of the adjacent a_1 and b_2 modes.[19(a)] On the other hand, some recent reports suggest

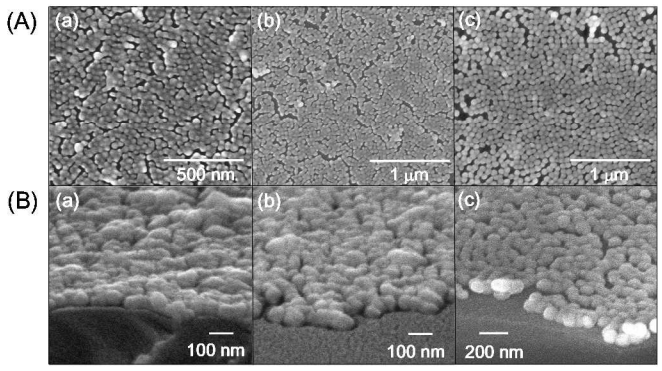

Figure 6. SEM images of the Au/AgNS assemblies. (A) Top views and (B) cross-sectional views of the assemblies of Au/AgNSs with the diameters of (a) 38 nm, (b) 53 nm, and (c) 90 nm.

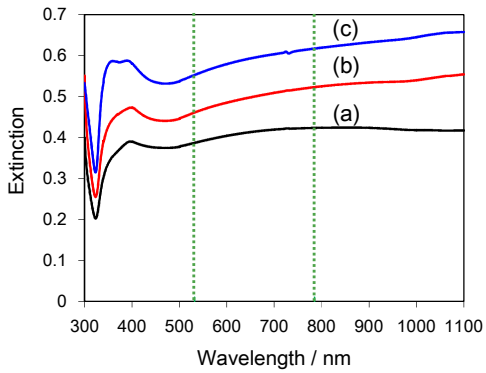

Figure 7. Extinction spectra of the assemblies of the Au/AgNSs with the diameters of (a) 38 nm, (b) 53 nm, and (c) 90 nm. Green-dotted lines indicate the excitation wavelengths in SERS measurements.

that *p,p'*-dimercaptoazobenzene (DMAB) is formed from PATP via N-N coupling induced by LSPR excitation. All of the above mentioned peaks are due to a_g modes of the DMAB.[28] Figure 8(B) shows the SERS spectra recorded at an excitation wavelength of 785 nm. The SERS signals of the PATP-modified 2-D assemblies are as pronounced as in the SERS spectra recorded upon excitation at 532 nm.

In order to quantify the enhancement of the Raman signals for each of the assemblies, we estimated the enhancement factors (EFs) using the following equation (1):[29]

$$\mathrm{EF} = \frac{I_{\mathrm{SERS}}/N_{\mathrm{surf}}}{I_{\mathrm{bulk}}/N_{\mathrm{bulk}}} \quad (1)$$

where I_{SERS} is the intensity of a vibrational mode in the SERS spectrum of PATP and I_{bulk} is the intensity of the same vibrational mode in the normal Raman spectrum of a methanol solution of PATP (10 M). In this study, the peak at ~1068 cm^{-1} ($7a_1$ mode) was selected for the calculation of the EF values since the a_1 vibrational mode is largely associated with the electromagnetic effect.[30] N_{surf} and N_{bulk} are the number of PATP molecules that are effectively excited by laser radiation on the nanoparticle assemblies and in solution phase, respectively. The detailed calculation of these parameters was described in the Supplementary Information and in our previous report.[11]

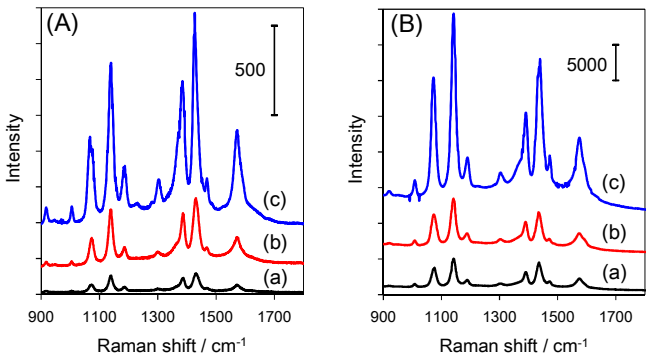

Figure 8. SERS spectra of PATP-modified assemblies of Au/AgNSs with the diameters of (a) 38 nm, (b) 53 nm, and (c) 90 nm measured at excitation wavelengths of (A) 532 nm and (B) 785 nm.

Table 1 Enhancement factors of the SERS peak at ~1068 cm^{-1} of PATP on assemblies of Au/AgNSs measured at the excitation wavelengths of 532 and 785 nm.

Sample	Au/AgNP(38)	Au/AgNP(53)	Au/AgNP(90)
EF at 532 nm	1.55×10^4	3.80×10^4	9.19×10^4
EF at 785 nm	2.38×10^5	4.37×10^5	1.90×10^6

The calculated EF values of the SERS intensities are shown in Table 1. At the excitation wavelengths of 532 and 785 nm, we observed strong enhancements of the Raman signal of PATP. It has been reported that the Raman signals of probe molecules were dramatically enhanced by the hot spots, which results from the coupling of the LSPR generated on the aggregated metal nanoparticles.[26(b),(c)] In this study, both the laser wavelengths (532 nm and 785 nm) overlapped with the longitudinal coupling modes of the Ag LSPR (see Figure 7), which makes it reasonable to assume that these enhancements are due to the generation of hot spots. These results suggest that the multiple hot spots produced by a longitudinal plasmon coupling at the interparticle junctions in the dense 2-D nanoparticle assemblies cause a drastic SERS enhancement.[26(d),31] Interestingly, the EFs dramatically increased with an increasing nanoparticle diameter, as revealed in Table 1. The EF values of Au/AgNS(90) assemblies were 5.9 and 8.0 times larger than those of Au/AgNS(36) at the excitation wavelengths of 532 and 785 nm, respectively.

Here we will discuss possible factors leading to the dependence of the EFs of SERS on the nanoparticle diameter that we have found as described above. One might argue that the number of PATP probe molecules may be different depending on the nanoparticle diameter. However, a simple geometric argument indicates that the total surface area of 2-D close-packed spheres is independent of the diameter of the sphere. Since each of our 2-D assemblies is almost close-packed as described in Section 3-2, we can safely assume that the number of PATP molecules immobilized on each of the assemblies does not differ significantly.

In the case that the resonance wavelength is shifted depending on the nanoparticle diameter, as reported for Au/AgNSs dispersed in solution, the EFs may vary with the wavelength of excitation because degree of the overlapping between the excitation wavelength and the resonance wavelength is different depending on the nanoparticle diameter. In the present case, however, this is irrelevant because the shape and position of the excitation spectra are constant for the range of nanoparticle sizes studied (Figure 7). Indeed, the SERS activity increased with increasing nanosphere diameter for both laser wavelength (532 and 785 nm). We therefore believe that the EFs of SERS must be governed by the electromagnetic effects in our assemblies.

There are some reports that studied the dependence of SERS activity on the diameter of nanospheres dispersed in solution. An optimal diameter of ~50 nm was found for Ag nanosphere in solution.[13(b)] An increase in the Ag nanoparticle size induces not only an increase in the local electromagnetic field but also in scattering, which disfavors the SERS signals. Another group reported that the SERS activity of the aggregates of Ag nanospheres in solution decreased with increasing nanosphere diameter.[13(c)] For Au/AgNSs well-dispersed in solution, an increase in the SERS activity with increase in the size of nanospheres was observed.[13(a)] This behavior could be explained by the generation of higher electromagnetic fields by particles with larger size.

The present nanosphere assemblies differ from these previously reported systems in that the assemblies are densely arranged 2-D assemblies and thus hot spots should play a major role in producing the large SERS activity. Even though the density of hot spots should be smaller for assemblies of nanospheres with a larger diameter, the observed SERS activity was higher for larger nanospheres. This new finding that increasing nanosphere diameter leads to dramatic enhancement of the SERS activity in the case of organized 2-D assemblies warrants further mechanistic studies to better understand the SERS phenomena in the nanoparticle assemblies.

Conclusions

Densely arranged two-dimensional assemblies of size-controlled Au(core)/Ag(shell) type nanospheres were easily fabricated by an organic solvent-mediated liquid-liquid interface assembly technique. We investigated the nanosphere size dependence of the SERS activity of the nanosphere assemblies using p-aminothiophenol as a probe molecule with excitation laser wavelengths of 532 and 785 nm. The 785 nm laser, which were effectively excites the hot spots, shows a stronger SERS activity and the enhancement factor increases with increasing the diameter of the assembled particles. This is of high importance for the development of highly sensitive SERS sensor tips. The use of silver nanoparticles with an optimized morphology promises to yield even larger enhancement factors, which is currently under research in our group.

Notes and references

[a] *College of Science and Technology, Nihon University, 1-8-14 Kanda Surugadai, Chiyoda-ku, Tokyo 101-8308, Japan.*
E-mail: sugawa.kosuke@nihon-u.ac.jp
[b] *Department of Materials Science, School of Engineering, The University of Shiga Prefecture, 2500 Hassaka-cho, Hikone-City, Shiga 522-8533, Japan.*
[c] *Department of Material Science and Technology, Tokyo University of Science, 6-3-1 Niijuku, Katsushika-ku, Tokyo 125-8585, Japan.*
[d] *Polymer Materials Unit, National Institute of Materials Science (NIMS), 1-1 Namiki, Tsukuba, Ibaraki 305-0044, Japan.*

Electronic Supplementary Information (ESI) available: [detailed calculation of enhancement factors of SERS]. See DOI: 10.1039/b000000x/

1. (a) S. Schlücker, *Angew. Chem. Int. Ed.*, 2014, **53**, 4756-4795. (b) W. Xie, S. Schlücker, *Phys. Chem. Chem. Phys.*, 2013, **15**, 5329-5344. (c) M. Vendrell, K. K. Maiti, K. Dhaliwal, Y.-T. Chang, *Trends Biotechnol.*, 2013, **31**, 249-257.
2. (a) A. Otto, I. Mrozek, H. Grabhorn and W. Akemann, *J. Phys. Condens. Matter.*, 1992, **4**, 1143-1212. (b) M. Moskovits, *Rev. Mod.*

Phys., 1985, **57**, 783-826. (c) G. C. Schatz, *Acc. Chem. Res.*, 1984, **17**, 370-376. (d) A. Campion and P. Kambhampati, *Chem. Soc. Rev.*, 1998, **27**, 241.

3. (a) S. Nie and S. R. Emory, *Science*, 1997, **275**, 1102-1106. (b) K. Kneipp, Y. Wang, H. Kneipp, L. T. Perelman, I. Itzkan, R. R. Dasari and M. S. Feld, *Phys. Rev. Lett.*, 1997, **78**, 1667-1670.
4. H. Xu, J. Aizpurua, M. Käll, P. Apell, *Phys. Rev. E: Stat. Phys., Plasmas, Fluids, Relat. Interdiscip. Top.*, 2000, **62**, 4318-4324. (b) L. Xia, M. Chen, X. Zhao, Z. Zhang, J. Xia, H. Xu and M. Sun, *J. Raman Spectrosc.*, 2014, **45**, 533-540.
5. (a) H. Xu, J. Aizpurua, M. Käll and P. Apell, *Phys. Rev. E*, 2000, **62**, 4318-4324. (b) V. I. Shautsova, V. A. Zhuravkov, O. V. Korolik, A. G. Novikau, G. P. Shevchenko and P. I. Gaiduk, *Plasmonics*, 2014, **9**, 993-999.
6. C. J. L. Constantino, T. Lemma, P. A. Antunes and R. Aroca, *Anal. Chem.*, 2001, **73**, 3674-3678.
7. M. Rycenga, C. M. Cobley, J. Zeng, W. Li, C. H. Moran, Q. Zhang, D. Qin and Y. Xia, *Chem. Rev.*, 2011, **111**, 3669-3712.
8. R. P. Van Duyne, J. C. Hulteen and D. A. Treichel, *J. Chem. Phys.*, 1993, **99**, 2101-2115.
9. (a) H. K. Lee, Y. H. Lee, Q. Zhang, I. Y. Phang, J. M. R. Tan, Y. Cui and X. Y. Ling, *ACS Appl. Mater. Interfaces*, 2013, **5**, 11409-11418. (b) N. Ahamad and A. Ianoul, *J. Phys. Chem. C*, 2011, **115**, 3587-3594. (c) M. A. Mahmoud, C. E. Tabor and M. A. El-Sayed, *J. Phys. Chem. C*, 2009, **113**, 5493-5501.
10. M. Fan and A. G. Brolo, *Phys. Chem. Chem. Phys.*, 2009, **11**, 7381-7389.
11. Y. Tanoue, K. Sugawa, T. Yamamuro and T. Akiyama, *Phys. Chem. Chem. Phys.*, 2013, **15**, 15802-15805.
12. (a) Q. Shao, R. Que, L. Cheng and M. Shao, *RSC Adv.*, 2012, **2**, 1762-1764. (b) A. Sánchez-Iglesias, P. Aldeanueva-Potel, W. Ni, J. Pérez-Juste, I. Pastoriza-Santos, R. A. Alvarez-Puebla, B. N. Mbenkum and L. M. Liz-Marzán, *Nano Today*, 2010, **5**, 21-27. (c) J.-C. Bian, Z. Li, Z.-D. Chen, H.-Y. He, X.-W. Zhang, X. Li and G.-R. Han, *Appl. Surf. Sci.*, 2011, **258**, 1831-1835. (d) J. J. Giner-Casares, L. M. Liz-Marzán, *Nano Today*, 2014, **9**, 365-377.
13. (a) A. K. Samal, L. Polavarapu, S. Rodal-Cedeira, L. M. Liz-Marzán, J. Pérez-Juste and I. Pastoriza-Santos, *Langmuir*, 2013, **29**, 15076-15082. (b) K. G. Stamplecoskie and J. C. Scaiano, *J. Phys. Chem. C*, 2011, **115**, 1403-1409. (c) C. S. Seney, B. M. Gutzman and R. H. Goddard, *J. Phys. Chem. C*, 2009, **113**, 74-80. (d) N. R. Jana, *Analyst*, 2003, **128**, 954-956.
14. Y. Ma and Y. Qu, *Nanoscale*, 2012, **4**, 3036-3039.
15. D. D. Evanoff, Jr. and G. Chumanov, *J. Phys. Chem. B*, 2004, **108**, 13948-13956.
16. (a) N. G. Bastús, J. Comenge and V. Puntes, *Langmuir*, 2011, **27**, 11098-11105. (b) J. Kimling, M. Maier, B. Okenve, V. Kotaidis, H. Ballot and A. Plech, *J. Phys. Chem. B*, 2006, **110**, 15700-15707.
17. J. Turkevich, P. C. Stevenson and J. Hillier, *Discuss. Faraday Soc.*, 1951, **11**, 55-75.
18. (a) M. Suzuki, Y. Niidome, N. Terasaki, K. Inoue, Y. Kuwahara and S. Yamada, *Jpn. J. Appl. Phys.*, 2004, **43**, L554-L556. (b) T. Akiyama, M. Nakada, N. Terasaki and S. Yamada, *Chem. Commun.*, 2006, 395-397. (c) K. Sugawa, T. Akiyama, H. Kawazumi and S. Yamada, *Langmuir*, 2009, **25**, 3887-3893. (d) K. Sugawa, T. Kawahara, T. Akiyama and S. Yamada, *Jpn. J. Appl. Phys.*, 2009, **48**, 04C132-1-04C132-5.
19. (a) Y.-F. Huang, D.-Y. Wu, H.-P. Zhu, L.-B. Zhao, G.-K. Liu, B. Ren and Z.-Q. Tian, *Phys. Chem. Chem. Phys.*, 2012, **14**, 8485-8497. (b) L.-B. Zhao, R. Huang, Y.-F. Huang, D.-Y. Wu and B. J. Ren, *J. Chem. Phys.,* 2011, **135**, 134707-1-134707-11.
20. D. P. Woodruff, *Phys. Chem. Chem. Phys.*, 2008, **10**, 7211-7221.
21. X. Liu, M. Atwater, J. Wang, Q. Huo, *Colloids Surf B Biointerfaces*, 2007, **58**, 3-7.
22. (a) S. Link and M. A. El-Sayed, *J. Phys. Chem. B*, 1999, **103**, 8410-8426. (b) J. D. Driskell, R. J. Lipert and M. D. Porter, *J. Phys. Chem. B*, 2006, **110**, 17444-17451. (c) S. K. Ghosh and T. Pal, *Chem. Rev.*, 2007, **107**, 4797-4862. (d) J. Zhao, A. O. Pinchuk, J. M. Mcmahon, S. Li, L. K. Ausman, A. L. Atkinson and G. C. Schatz, *Acc. Chem. Res.*, 2008, **41**, 1710-1720.
23. U. Kreibig and M. Vollmer, "Optical Properties of Metal Clusters", Springer Series in Materials Science 25; Springer-Verlag: New York, 1995.
24. C. A. Schneider, W. S. Rasband, K.W. Eliceiri, *Nat. Methods*, 2012, **9**, 671-675.
25. P. J. G. Goulet, D. S. dos Santos, Jr., R. A. Alvarez-Puebla, O. N. Oliveira, Jr. and R. F. Aroca, *Langmuir*, 2005, **21**, 5576-5581.
26. (a) J. M. McMahon, S. Li, L. K. Ausman and G. C. Schatz, *J. Phys. Chem. C*, 2012, **116**, 1627-1637. (b) J. P. Camden, J. A. Dieringer, Y. Wang, D. J. Masiello, L. D. Marks, G. C. Schatz and R. P. Van Duyne, *J. Am. Chem. Soc.*, 2008, **130**, 12616-12617. (c) K. L. Wustholz, A.-I. Henry, J. M. McMahon, R. G. Freeman, N. Valley, M. E. Piotti, M. J. Natan, G. C. Schatz and R. P. Van Duyne, *J. Am. Chem. Soc.*, 2010, **132**, 10903-10910. (d) A. Chen, A. E. DePrince III, A. Demortière, A. Joshi-Imre, E. V. Shevchenko, S. K. Gray, U. Welp and V. K. Vlasko-Vlasov, *Small*, 2011, **7**, 2365-2371.
27. (a) M. Osawa, N. Matsuda, K. Yoshii and I. Uchida, *J. Phys. Chem.*, 1994, **98**, 12702-12707. (b) Y. Wang, X. Zou, W. Ren, W. Wang and E. Wang, *J. Phys. Chem. C*, 2007, **111**, 3259-3265.
28. (a) Y. Fang, Y. Li, H. Xu and M. Sun, *Langmuir*, 2010, **26**, 7737-7746. (b) M. Sun and H. Xu, *Small*, 2012, **8**, 2777-2786.
29. (a) W. B. Cai, B. Ren, X. Q. Li, C. X. She, F. M. Liu, X. W. Cai and Z. Q. Tian, *Surf. Sci.*, 1998, **406**, 9-22. (b) E. J. Smythe, M. D. Dickey, J. Bao, G. M. Whitesides and F. Capasso, *Nano Lett.*, 2009, **9**, 1132-1138.
30. Q. Zhou, Y. Chao, Y. Li, W. Xu, Y. Wu and J. Zheng, *ChemPhysChem*, 2007, **8**, 921-925.
31. W. Lee, S. Y. Lee, R. M. Briber and O. Rabin, *Adv. Funct. Mater.*, 2011, **21**, 3424-3429.